Mass Spectrometry Imaging of Cholesterol and Oxysterols

William J Griffiths, Eylan Yutuc and Yuqin Wang

Swansea University Medical School, Singleton Park, Swansea, SA2 8PP, Wales, UK

Email, w.j.griffiths@swansea.ac.uk, eylan.yutuc@swansea.ac.uk, y.wang@swansea.ac.uk

Abstract

Mass spectrometry imaging (MSI) is a new technique in the toolbox of the analytical biochemist. It allows the generation of a compound specific image from a tissue slice where a measure of compound abundance is given pixel by pixel, usually displayed on a colour scale. As mass spectra are recorded at each pixel the data can be interrogated to generate images of multiple different compounds all in the same experiment. Mass spectrometry (MS) requires ionisation of analytes but cholesterol and other neutral sterols tend to be poorly ionised by the techniques employed in most MSI experiments, so despite its high abundance in mammalian tissues cholesterol is poorly represented in the MSI literature. In this article we discuss some of the MSI studies where cholesterol has been imaged and introduce newer methods for its analysis by MSI. Disturbed cholesterol metabolism is linked to many disorders and the potential of MSI to study cholesterol, its precursors and its metabolites in animal models and from human biopsies will be discussed.

Key words: Mass spectrometry, mass spectrometry imaging, cholesterol, oxysterol, neurodegeneration, 24S-hydroxycholesterol

Introduction

Pioneering work by the groups of Caprioli, Spengler, Clench and Murphy has moved mass spectrometry imaging (MSI) from the preserve of the mass spectrometry (MS) specialist into the realm of the analytical biochemist (1-4). At its simplest, a probe (e.g., laser or ion beam) samples the surface of a tissue section pixel by pixel with mass spectra being recorded of the sampled-surface at each pixel. An image of any ion recorded by the MS can then be generated across the sampled surface with ion abundance pixel by pixel illustrated on a colour scale (Figure 1) (5, 6). As an ion's *mass/charge* (*m/z*), as recorded by MS, is related to its parent compound's molecular mass, and hence to a particular compound, MSI at least to a first approximation, gives a molecular image of a compound in a tissue. There are many differing sampling probes providing different degrees of spatial resolution, ranging from 100 to 400 nm or smaller for secondary ion mass spectrometry (SIMS) at the high spatial resolution end of the spectrum (7, 8); 50 to 100 µm typical for matrix-assisted laser desorption ionisation (MALDI) (4-6) and desorption electrospray ionisation ionisation (DESI) (9) and 20 µm or less for the more sensitive MALDI2 (10, 11); to 300 - 1,000 µm for liquid extraction for surface analysis (LESA) at the low spatial resolution end of the spectrum (12, 13). However, as spatial resolution is increased the pixel size get smaller and the available tissue to be analysed is reduced meaning that low-abundance metabolites are discriminated against at high spatial resolution, this is less of a problem for highly abundant cholesterol but is for its lower abundance precursors and metabolites.

A challenge for MSI of sterols is their comparatively poor ionisation characteristics in MALDI-MSI and DESI-MSI, two of the dominating MSI technologies of today (4, 9). Phospholipids are more readily ionised and tend to dominate the MSI spectra of animal tissues. Cholesterol is usually observed as the $[M+H-H_2O]^+$ ion at *m/z* 369.35 and cannot be differentiated from its isomers lathosterol or zymostenol (Figure 2), although the latter two isomers are almost always of very minor abundance in comparison to cholesterol and unlikely to significantly contribute to the signal at *m/z* 369.35 (14). Isomer differentiation is more of a problem for desmosterol, 7-dehydrocholesterol (7-DHC) and 8-

dehydrocholesterol (8-DHC), precursors of cholesterol, often found in similar abundance in tissue, and can lead to misidentifications found in the literature. MSI of oxysterols (oxidised forms of cholesterol) is even more challenging on account of the fact that they can be formed *in vivo* from cholesterol enzymatically and non-enzymatically but also *ex vivo* in air (15), and tissue sections for MSI are prepared in air. The situation is further complicated in that oxysterols formed *ex vivo* are isomeric to those formed *in vivo* and most MSI technologies are unable to resolve isomers. Despite these challenges for the analysis of sterols and oxysterols technologies are being developed to allow their imaging.

MALDI-MSI and DESI-MSI of cholesterol and its precursors

Both MALDI and DESI are desorption ionisation methods (5). In MALDI-MSI the tissue section to be analysed is coated with matrix, usually a UV absorbing matrix, by spraying the matrix from a pneumatic sprayer or by sublimation of the matrix onto the tissue surface in a vacuum chamber. A matrix is not required for DESI. The tissue itself is usually of 5 – 20 µm thickness cryo-sectioned using a microtome. The tissue is thaw-mounted onto a microscope slide which often has a conductive surface of indium tin oxide for MALDI-MS (5). In the MALDI process the exact ionisation mechanism is still a subject of debate but can be imagined in simple terms as the excitation of the matrix by the absorption of laser light (usually 337, 349 or 355 nm) leading to vaporisation and ionisation of matrix and surface analytes, and in the positive ion mode the transfer of a cation, often a proton or alkali metal, from the matrix to the analyte. This mechanism favours the analysis of Brønsted and Lewis bases. In the negative-ion mode, the matrix acts as a Brønsted or Lewis base and ionisation favours proton donors. The ionisation process can occur under vacuum (vacuum MALDI) or at atmospheric pressure (AP-MALDI), but in both cases does not favour the ionisation of cholesterol in either the positive or negative-ion mode, as it is a weak proton accepter and weak proton donor. Never-the-less in tissues where cholesterol is abundant images can be generated. The brain is a good example of an organ rich in cholesterol with average levels about 20 µg/mg wet weight (16). MALDI-MSI has been used to image cholesterol in rodent brain and highlight its differential abundance in distinct anatomical regions (17, 18). Although aromatic small molecules usually constitute the MALDI matrix, graphene oxide has also been used in the MSI of cholesterol as the $[M-H]^-$ ion at *m/z* 385.35 in breast cancer tissue (Figure 3) (19).

Silver ions (Ag^+) are known to complex to double bonds (Figure 3) (20). This chemistry has been exploited for the MSI of sterols. In an early study, $AgNO_3$ was sprayed as a "matrix" onto an etched silicon wafer and tissue thaw mounted ready for "nano-structure initiator" – MSI (21). Images were generated for cholesterol as $[M + {}^{109}Ag]^+$ at *m/z* 495 and for dehydrocholesterol, a combination of 7-DHC (probably also 8-DHC) and desmosterol, at *m/z* 493 from brains of 1-day old mice. In brain tissue from a mouse model of Smith-Lemli-Opitz syndrome (SLOS), where *7-dehydrocholesterol reductase* (*Dhcr7*), the gene that codes the enzyme that converts 7-DHC to cholesterol, is deleted a build-up of dehydrocholsterols was observed in the cerebellum and brain stem (21). The application of Ag^+ to enhance MSI can be achieve in different way, $AgNO_3^+$ solution can be pneumatically sprayed onto tissue (22) or alternatively silver can be sputtered onto tissue (23, 24). The end result is the same, an improvement in the sensitivity for MSI of double bond containing sterols.

A modification of MALDI called MALDI-2 has been developed which improves the ionisation of certain lipid classes including sterols. Here a second laser pulse interacts with the plume of matrix and analyte generated by a primary laser producing more matrix ions available to transfer charge to analyte (10). Using MALDI-2 cholesterol, monitored as the $[M+H-H_2O]^+$ at 369.35 has been imaged in a sagittal section of rat brain and at high spatial resolution (15 µm) in mouse cerebellum, as has somewhat strangely vitamin D_3 as the $[M+H]^+$ ion *m/z* 385.35 (10, 11). Vitamin D_3 is the light-induced ring opened product of 7-DHC. Its presence in the circulation is extremely low and it is unlikely to be present in

brain. It is more likely that the authors were detecting 7-DHC, 8-DHC, their isomer desmosterol or a dehydrated cholesterol autoxidation product or perhaps vitamin D_3 artifactually generated by laser light (Figure 2). Interestingly, MALDI-2 has been used to image cholesterol esters in multiple sclerosis brain tissue at the small pixel size of 6 µm (5). Cholesterol esters, if present in mammalian brain are present at very low levels (16), but perhaps their presence in multiple sclerosis brain is a consequence of the disease itself.

Like MALDI, DESI is a desorption ionisation method. In DESI an electrospray of charged solvent droplets is directed at the target surface, the charged droplets sample the surface extracting analytes and scatter in the direction of the inlet capillary of the mass spectrometer. Ionisation occurs in an ESI-like process with analytes having a high gas phase basicity being most preferentially ionised in the positive ion mode and those with a high gas phase acidity being preferentially ionised in the negative-ion mode (25). DESI can be used for MSI with the dimensions of the primary electrospray beam dictating pixel size. Pixel sizes of 50 – 150 µm are most common. Due to its lack of strong basic or acidic groups cholesterol tends to be poorly ionised by DESI, however, ionisation can be improved by incorporating trifluoroacetic acid in the DESI spray solvent (9). DESI-MSI has been nicely exploited for the imaging of mouse brain and in a mouse model of Alzheimer's disease (AD) (9). Infra-red (IR)– MALD-ESI is a hybrid of IR-MALD and ESI where analytes are desorbed by IR-MALD and ionisation achieved in a plume of charged droplets from an ESI emitter. Using IR-MALD-ESI-MSI cholesterol has been imaged in skin and found to be high in the epidermis (26).

MSI of sterols exploiting chemical derivatisation

The concept of derivatisation is embedded in the history of sterol/steroid analysis (27). Although primarily used to enable gas-chromatography – MS of sterols/steroids, derivatisation has also been employed to improve the sensitivity of LC-MS and MALDI-MS analysis (28). More recently derivatisation methods have been used to enhance MSI of sterols/steroids (29, 30). Many steroids possess a keto (oxo) group, this function is readily derivatised by hydrazine reagents to give a hydrazone, and this form of derivatisation has been widely exploited in steroid biochemistry for decades to enhance substrate polarity (Figure 4) (31, 32). Two popular derivatisation reagents are the Girard T (GT) and Girard P (GP) reagents which contain a positively charged nitrogen group, these have been used for on-tissue derivatisation to enhance the signals for steroids in a number of different tissues. The derivatisation reagent can be sprayed onto a tissue slice using a pneumatic sprayer then incubated in an acidic atmosphere to catalyse the reaction, and after drying in a desiccator and application of matrix, is ready for MALDI-MSI or in the absence of matrix DESI-MSI. This form of technology has been used for MSI of steroids in rodent adrenal tissue (33, 34), testis (35, 36), lung (37), cartilage (38), tumour xenografts (39) and brain (40).

Cholesterol and most oxysterols, however, do not possess an oxo group and are not suitable for direct derivatisation with hydrazine reagents. This obstacle is overcome for in-solution derivatisation by incorporating an enzymatic oxidation step prior to treatment with Girard reagent (41, 42), and can be similarly adopted as part of the on-tissue derivatisation approach (6, 43). This on-tissue "enzyme-assisted derivatisation for sterol analysis" (EADSA) approach has been successfully adopted for imaging cholesterol in rodent and human brain, liver tissue and in the developing zebrafish. In brief, fresh frozen tissue from e.g. rodent brain is cryo-sectioned to 10 – 15 µm thickness and thaw-mounted onto glass slides (ITO coated for MALDI-MSI) and dried in a vacuum desiccator, then isotope-labelled standards in ethanol are pneumatically sprayed onto the tissue to allow for normalisation of signal. Bacterial cholesterol oxidase is next sprayed onto the tissue in phosphate buffer, the tissue is then incubated for 1 hr in a humid atmosphere. Cholesterol oxidase enzyme oxidises 3β-hydroxy-5-ene sterols to their 3-oxo-4-ene analogues (Figure 4) (44), and after drying the tissue again in a desiccator

it is sprayed with GP reagent in aqueous acidic methanol, then incubated in an atmosphere of aqueous acidic methanol (6, 43). The tissue is dried once more. For MALDI-MSI matrix is sprayed onto tissue prior to analysis, this is not required for DESI-MSI or LESA-MSI (see below).

Shown in Figure 5 (top panel) is an image of cholesterol in a sagittal section of mouse brain, generated following on-tissue EADSA. This image can be matched to plate 17 of the Allen Mouse Brain Atlas https://mouse.brain-map.org/static/atlas (Figure 5, bottom panel) (45). The image was recorded at 50 µm resolution using AP-MALDI with *m/z* measurement to an accuracy of 10 ppm on an Orbitrap IDX mass spectrometer. Cholesterol is seen to be abundant in fibre tracts, particularly those of the corpus callosum, arbor vitae of the cerebellum and of pons and medulla (see https://mouse.brain-map.org/static/atlas). Images with higher spatial resolution can be recorded but with the penalty of acquisition time. Here the assumption is made that the ion at 518.4105 ± 10 ppm (Figure 5, top panel) corresponds to cholesterol, this is reasonable as its isomers lathosterol and zymostenol are of much lower abundance in brain (14). An added advantage of Girard derivatisation is that the derivatised sterols give informative fragmentation patterns in tandem MS (MS/MS or MS^2) and even more information when multistage fragmentation is applied (MS^n) (46). Where available this allows the use of MS^3 to generate an image in MALDI-MSI and to confirm that the ion being monitored is in fact derived from cholesterol (Figure 6) (6, 30). A problem encountered in MALDI-MSI is that tissue surface is exposed to air during sample preparation, this is almost unavoidable as the tissue needs to be cryo-sectioned and manually mounted on a slide. Exposure to air can lead to oxidation of cholesterol and the artefactual formation of an oxysterol. This makes MALDI-MSI of oxysterols almost impossible unless a fragment ion can be found that is unique to an endogenous oxysterol and absent from MS/MS or MS^n spectra of autoxidation artefacts, in which case MALDI-MSI could be carried out using a multiple-reaction monitoring (MRM) like "scan".

A way to circumvent the problem of distinguishing endogenous compounds from isomers potentially formed by autoxidation is to introduce a separation step between surface-sampling and mass spectrometry analysis. One possibility is ion mobility separation, where after ionisation ions are separated based on their size, shape and charge (47), however, this has yet to show separation of sterol isomers. A different strategy is to decouple surface-sampling from MS analysis. We have recently taken this approach where the surface is sampled by a robotic probe as in the LESA technique (12, 13), and the extracted analytes separated by LC prior to ESI-MS analysis (43). We have adopted this strategy following on-tissue EADSA to image mouse brain using a grid format where each pixel corresponds to a LESA-extraction followed by LC separation and MS(MS^n) analysis (43). Pixel size can be 300 µm, but the penalty of chromatographic resolution is in analysis time where each LESA-LC-MS(MS^n) run may take 1 hr, hence spatial resolution is usually degraded to 800 µm requiring fewer pixels to cover a mouse brain section, which is the order of about 100 pixels at 800 µm resolution (Figure 7). Despite the long analysis time and comparatively low resolution a surface can be imaged for individual oxysterol isomers and for cholesterol and its precursors all in a single analysis (43). Shown in Figure 7 is the layout for pixel by pixel analysis of a sagittal section of mouse brain and the resulting images for 24S-hydroxycholesterol (24S-HC), 24S,25-epoxycholesterol (24S,25-EC), cholesterol and its precursors desmosterol and 7-DHC/8-DHC. These images correspond to plate 17 in the Allen Mouse Brain Atlas (see https://mouse.brain-map.org/static/atlas). Note the nose is absent from the tissue section analysed and the pixels in the far left column are likely to have been over-sampled due to tissue folding during the mounting process. Never-the-less, 24S-HC is found to be most abundant in the thalamus and stratum regions of mouse brain while cholesterol is most abundant in the pons and medulla (Figure 7) (43). The LESA-LC-MSI method incorporating GP-derivatisation has recently been used to support PET imaging studies of CYP46A1, the enzyme that converts cholesterol to 24S-HC in brain (48).

An alternative route for on-tissue derivatisation of sterols is to exploit chemical derivatisation of the sterol hydroxy group to a ketone followed by derivatisation with hydrazine reagent and MALDI-MSI (49) or to derivatise the hydroxy group directly with betaine aldehyde. The latter has been use for DESI-MSI where betaine aldehyde is included in the ESI spray solvent (50).

Secondary Ion Mass Spectrometry (SIMS) – MSI

SIMS provides highest spatial resolution MSI. Here a fast moving ion beam (keV) of metal ions or clusters e.g. C_{60}^+, are focused to give a pixel size of less than 1 µm and results in surface ionisation. Primary ion beams tend to lead to high fragmentation of lipids which is a disadvantage for MSI (5). NanoSIMS is a variant of SIMS which uses Cs^+ or O^- as the primary ion beam leading to extensive fragmentation of lipids on the tissue surface but spatial gives resolutions of 50 – 100 nm (7). A clever application of NanoSIMS is where cells are enriched with ^{18}O-cholesterol by culturing in medium containing ^{18}O-cholesterol. The cells are then analysed by NanoSIMS and the $^{18}O^-$ fragment ion monitored (7). As plasma membranes are rich in cholesterol it can be assumed that when imaging these membranes the $^{18}O^-$ ions detected are derived from the labelled cholesterol. By incubating fibroblasts with both ^{18}O-cholesterol and ^{15}N-sphingosine and ^{15}N-sphingonine Kraft and colleagues could show that plasma membranes contain domains enriched in ^{15}N-sphingolipids but that ^{18}O is more uniformly distributed, indicating that sphingolipids and cholesterol do not form domains rich in both cholesterol and sphingolipids (51). This argues against the lipid raft hypothesis (52).

When SIMS uses a liquid metal ion gun filled with bismuth a primary beam of Bi_3^+ cluster ions is generated which provide a softer form of ionisation with $[M+H]^+$ and $[M+H-H_2O]^+$ ions being generated from a tissue surface. Lazar et al used this form of SIMS-MSI to image cholesterol in brain tissue from human donors and found that cholesterol is elevated in cortical layers III and IV of the cerebral cortex of tissue from AD donors (8).

Potential use of MSI to study the involvement of sterols in disease

For many years disordered cholesterol metabolism has been linked with neurodegenerative disease including AD, Huntington's disease, Parkinson's disease, motor neuron disease and multiple sclerosis (53-57). MSI provides an exciting tool to investigate these disorders both from human donors and mouse models. However, most of the cholesterol in brain is located in the myelin sheaths (70 – 80 % in rat and mouse brain) surrounding axons and is metabolically inactive (16), so while gross changes in oligodendrocyte cholesterol are likely to be detected by MSI e.g. in multiple sclerosis, this is unlikely to be so for metabolically active cholesterol in neurons. MSI for cholesterol precursors and metabolites may prove a better approach to study neurodegenerative disorders. However, cholesterol precursors and metabolites are about 100 – 1000 times lower abundance than cholesterol in brain making their imaging a challenge (58). Perhaps the LESA-LC-MSI approach incorporating derivatisation will prove most successful as this allows cholesterol its immediate precursors and metabolites to be analysed in brain in a single assay, although admittedly at low spatial resolution (43).

Sterols are not only implicated in neurodegeneration, but also fatty liver and diabetes, atherosclerosis and inflammatory disorders. MSI will no doubt be used in the study of these diseases and provide much needed correlation between sterol concentrations and location.

Conclusion

MSI has a great potential for the analysis of sterols and oxysterols and in investigations of their importance to human health. While most of the studies to date have been performed on rodent models, human tissue can also be analysed. The major advantage of MSI is that when utilised with

appropriate isotope labelled standards absolute concentrations of analytes can be determined at defined anatomical locations. While it is possible to generate images of cholesterol at sub-µm pixel sizes, MSI of less abundant sterols and oxysterols is more challenging, the challenge is accentuated by the existence of multiple oxysterol isomers and the prevalence of cholesterol to become oxidised *ex vivo* in air to give oxysterols of identical structure to those generated *in vivo*. Never-the-less separation methods are being developed to link with MSI which will allow isomer separation although the problem of autoxidation may be more difficult to overcome. A major advantage of MSI is that besides the analyte of interest images can be generated for other molecules that ionise and are recorded in the MS scan. From a health perspective we foresee MSI to offer real advantages in the study of neurodegenerative disease, fatty liver and diabetes and in the field of immunity.

Acknowledgements

We are indebted to Drs Joyce Yau, Shazia Khan and Ruth Andrew from the University of Edinburgh for providing mouse brain tissue. We thank Drs Lauren Griffiths and Roberto Angelini for their work on MALDI-MSI in Swansea and Dr Malcolm Clench, Sheffield Hallam University, for inspiring us to join the MSI field. This work was supported by BBSRC, part of UKRI. Members of the European Network for Oxysterol Research (ENOR, https://www.oxysterols.net/) are thanked for informative discussions.

Declaration of competing interests

The authors declare the following financial interests which may be considered as potential competing interests: WJG and YW are listed as inventors on the patent "Kit and method for quantitative detection of steroids" US9851368B2. WJG, EY and YW are shareholders in CholesteniX Ltd.

Figure Captions

Figure 1. Schematic of MSI. A probe e.g. laser light or an ion-beam, samples the surface of a tissue section pixel by pixel. Mass spectra are recorded at each pixel. An image of any recorded ion is generated from its MS-abundance data at each pixel. MALDI-MSI of the $[M+H-H_2O]^+$ of cholesterol in a sagittal section of mouse brain is illustrated. Modified from Angelini et al, Analytical Chemistry 2021 93 (11), 4932-4943, reference (6),

Figure 2. Structures of cholesterol, desmosterol and their isomers, and of the oxysterols 24S-hydroxycholesterol formed enzymatically and of 7α-hydroxycholesterol and 7β-hydroxycholesterol which can both be formed *in vivo* enzymatically or non-enzymatically and *ex vivo* by autoxidation. The structures of 6β-hydroxycholesterol and cholesta-5,6-epoxide are also shown.

Figure 3. Ionisation of cholesterol by MALDI, and of other double bond containing sterols by silver-laser desorption ionisation (AgLDI).

Figure 4. Derivatisation of steroids and sterols with the Girard T (GT) and Girard P (GP) reagents. To derivatise sterols without a keto (oxo) group but with a 3β-hydroxy group cholesterol oxidase is used to oxidise the hydroxy group to a ketone ready for subsequent reaction with Girard reagent.

Figure 5. AP-MALDI-MSI of cholesterol in a sagittal section mouse brain following on tissue EADSA with derivatisation using GP reagent. The upper panel shows the image of GP-derivatised cholesterol at *m/z* 518.4105 ± 10 ppm. The central panel depicts an optical image of the same tissue section, and the bottom panel is plate 17 from the Allen Mouse Brain Atlas https://mouse.brain-map.org/static/atlas (Allen Institute for Brain Science) (45).

Figure 6 . API-MALDI-MSI of cholesterol following GP derivatisation exploiting MS^3 targeting the cerebellum in a sagittal section of mouse brain. (A) MS^3 spectrum of endogenous cholesterol from a single pixel. (B) MS^3 spectrum of authentic cholesterol standard. (C) Image of cholesterol generated using the MS^3 transition 518→439→163. (D) Fragmentation pattern for GP-derivatised cholesterol. MB midbrain, P pons, MY medulla, CBX cerebellum. Modified from Angelini et al, Analytical Chemistry 2021 93 (11), 4932-4943, reference (6), Copyright © 2021 The Authors. Published by American Chemical Society under CC-BY licence.

Figure 7. LESA-LC-MSI of cholesterol its precursors and oxysterols after on-tissue EADSA with GP derivatisation. Identification of analytes was confirmed by retention time, accurate mass, MS^3 spectra and reference to authentic standards. Quantification was made by isotope dilution against isotope labelled sprayed-on standards. (A) Grid showing each pixel to be analysed in a sagittal section of mouse brain. (B) Plate 17 in the Allen Mouse Brain Atlas (Allen Institute for Brain Science) (see https://mouse.brain-map.org/static/atlas) (45). (C) 24S-hydroxycholesterol, (D) cholesterol, (E) 24S,25-epoxycholesterol, (F) desmosterol and (G) 7/8-DHC.

References

1. Stoeckli, M., P. Chaurand, D. E. Hallahan, and R. M. Caprioli. 2001. Imaging mass spectrometry: A new technology for the analysis of protein expression in mammalian tissues. *Nature Medicine* **7**: 493-496.
2. Spengler, B. 2015. Mass spectrometry imaging of biomolecular information. *Anal Chem* **87**: 64-82.
3. Trim, P. J., S. J. Atkinson, A. P. Princivalle, P. S. Marshall, A. West, and M. R. Clench. 2008. Matrix-assisted laser desorption/ionisation mass spectrometry imaging of lipids in rat brain tissue with integrated unsupervised and supervised multivariant statistical analysis. *Rapid Commun Mass Spectrom* **22**: 1503-1509.
4. Berry, K. A., J. A. Hankin, R. M. Barkley, J. M. Spraggins, R. M. Caprioli, and R. C. Murphy. 2011. MALDI imaging of lipid biochemistry in tissues by mass spectrometry. *Chem Rev* **111**: 6491-6512.
5. Ellis, S. R., and J. Soltwisch. 2023. Mass Spectrometry Imaging of Lipids. *In* Mass Spectrometry for Lipidomics. 117-150.
6. Angelini, R., E. Yutuc, M. F. Wyatt, J. Newton, F. A. Yusuf, L. Griffiths, B. J. Cooze, D. El Assad, G. Frache, W. Rao, L. B. Allen, Z. Korade, T. T. A. Nguyen, R. A. C. Rathnayake, S. M. Cologna, O. W. Howell, M. R. Clench, Y. Wang, and W. J. Griffiths. 2021. Visualizing Cholesterol in the Brain by On-Tissue Derivatization and Quantitative Mass Spectrometry Imaging. *Anal Chem* **93**: 4932-4943.
7. Brunet, M. A., and M. L. Kraft. 2023. Toward Understanding the Subcellular Distributions of Cholesterol and Sphingolipids Using High-Resolution NanoSIMS Imaging. *Accounts of Chemical Research* **56**: 752-762.
8. Lazar, A. N., C. Bich, M. Panchal, N. Desbenoit, V. W. Petit, D. Touboul, L. Dauphinot, C. Marquer, O. Laprévote, A. Brunelle, and C. Duyckaerts. 2013. Time-of-flight secondary ion mass spectrometry (TOF-SIMS) imaging reveals cholesterol overload in the cerebral cortex of Alzheimer disease patients. *Acta Neuropathologica* **125**: 133-144.
9. Wang, X., Y. Hou, Z. Hou, W. Xiong, and G. Huang. 2019. Mass Spectrometry Imaging of Brain Cholesterol and Metabolites with Trifluoroacetic Acid-Enhanced Desorption Electrospray Ionization. *Analytical Chemistry* **91**: 2719-2726.
10. Soltwisch, J., H. Kettling, S. Vens-Cappell, M. Wiegelmann, J. Muthing, and K. Dreisewerd. 2015. Mass spectrometry imaging with laser-induced postionization. *Science* **348**: 211-215.
11. Ellis, S. R., J. Soltwisch, M. R. L. Paine, K. Dreisewerd, and R. M. A. Heeren. 2017. Laser post-ionisation combined with a high resolving power orbitrap mass spectrometer for enhanced MALDI-MS imaging of lipids. *Chemical Communications* **53**: 7246-7249.

12. Almeida, R., Z. Berzina, E. C. Arnspang, J. Baumgart, J. Vogt, R. Nitsch, and C. S. Ejsing. 2015. Quantitative spatial analysis of the mouse brain lipidome by pressurized liquid extraction surface analysis. *Anal Chem* **87**: 1749-1756.
13. Hall, Z., Y. Chu, and J. L. Griffin. 2017. Liquid Extraction Surface Analysis Mass Spectrometry Method for Identifying the Presence and Severity of Nonalcoholic Fatty Liver Disease. *Anal Chem* **89**: 5161-5170.
14. Lütjohann, D., M. Stroick, T. Bertsch, S. Kühl, B. Lindenthal, K. Thelen, U. Andersson, I. Björkhem, K. v. Bergmann, and K. Fassbender. 2004. High doses of simvastatin, pravastatin, and cholesterol reduce brain cholesterol synthesis in guinea pigs. *Steroids* **69**: 431-438.
15. Schroepfer, G. J., Jr. 2000. Oxysterols: modulators of cholesterol metabolism and other processes. *Physiol Rev* **80**: 361-554.
16. Dietschy, J. M., and S. D. Turley. 2004. Thematic review series: brain Lipids. Cholesterol metabolism in the central nervous system during early development and in the mature animal. *J Lipid Res* **45**: 1375-1397.
17. Tobias, F., M. T. Olson, and S. M. Cologna. 2018. Mass spectrometry imaging of lipids: untargeted consensus spectra reveal spatial distributions in Niemann-Pick disease type C1. *J Lipid Res* **59**: 2446-2455.
18. Cologna, S. M. 2019. Mass Spectrometry Imaging of Cholesterol. *Adv Exp Med Biol* **1115**: 155-166.
19. Zhou, D., S. Guo, M. Zhang, Y. Liu, T. Chen, and Z. Li. 2017. Mass spectrometry imaging of small molecules in biological tissues using graphene oxide as a matrix. *Analytica Chimica Acta* **962**: 52-59.
20. Nikolova-Damyanova, B. 2009. Retention of lipids in silver ion high-performance liquid chromatography: facts and assumptions. *J Chromatogr A* **1216**: 1815-1824.
21. Patti, G. J., L. P. Shriver, C. A. Wassif, H. K. Woo, W. Uritboonthai, J. Apon, M. Manchester, F. D. Porter, and G. Siuzdak. 2010. Nanostructure-initiator mass spectrometry (NIMS) imaging of brain cholesterol metabolites in Smith-Lemli-Opitz syndrome. *Neuroscience* **170**: 858-864.
22. Yang, E., F. Fournelle, and P. Chaurand. 2020. Silver spray deposition for AgLDI imaging MS of cholesterol and other olefins on thin tissue sections. *Journal of Mass Spectrometry* **55**: e4428.
23. Xu, L., M. Kliman, J. G. Forsythe, Z. Korade, A. B. Hmelo, N. A. Porter, and J. A. McLean. 2015. Profiling and Imaging Ion Mobility-Mass Spectrometry Analysis of Cholesterol and 7-Dehydrocholesterol in Cells Via Sputtered Silver MALDI. *J Am Soc Mass Spectrom* **26**: 924-933.
24. Nezhad, Z. S., J. P. Salazar, R. S. Pryce, L. M. Munter, and P. Chaurand. 2022. Absolute quantification of cholesterol from thin tissue sections by silver-assisted laser desorption ionization mass spectrometry imaging. *Anal Bioanal Chem* **414**: 6947-6954.
25. Cooks, R. G., Z. Ouyang, Z. Takats, and J. M. Wiseman. 2006. Detection Technologies. Ambient mass spectrometry. *Science* **311**: 1566-1570.
26. Bai, H., K. E. Linder, and D. C. Muddiman. 2021. Three-dimensional (3D) imaging of lipids in skin tissues with infrared matrix-assisted laser desorption electrospray ionization (MALDESI) mass spectrometry. *Anal Bioanal Chem* **413**: 2793-2801.
27. Sjovall, J. 2004. Fifty years with bile acids and steroids in health and disease. *Lipids* **39**: 703-722.
28. Wang, Y., and W. J. Griffiths. 2020. CHAPTER 6 Derivatisation for Direct Infusion– and Liquid Chromatography–Mass Spectrometry. *In* Lipidomics: Current and Emerging Techniques. The Royal Society of Chemistry. 122-147.
29. Huang, S., X. Liu, D. Liu, X. Zhang, L. Zhang, W. Le, and Y. Zhang. 2022. Pyrylium-Based Derivatization for Rapid Labeling and Enhanced Detection of Cholesterol in Mass Spectrometry Imaging. *J Am Soc Mass Spectrom* **33**: 2310-2318.
30. Griffiths, W. J., E. Yutuc, D. Davies, A. Dickson, R. Angelini, D. El Assad, G. Frache, and Y. Wang. 2020. Lipidomics Basics. *In* Lipidomics: Current and Emerging Techniques. W. J. Griffiths and Y. Wang, editors. Royal Society of Chemistry, Cambridge. 1 - 24.

31. Girard, A., and G. Sandulesco. 1936. Sur une nouvelle série de réactifs du groupe carbonyle, leur utilisation à l'extraction des substances cétoniques et à la caractérisation microchimique des aldéhydes et cétones. *Helvetica Chimica Acta* **19**: 1095-1107.
32. Wheeler, O. H. 1968. The Girard reagents. *Journal of Chemical Education* **45**.
33. Takeo, E., Y. Sugiura, T. Uemura, K. Nishimoto, M. Yasuda, E. Sugiyama, S. Ohtsuki, T. Higashi, T. Nishikawa, M. Suematsu, E. Fukusaki, and S. Shimma. 2019. Tandem Mass Spectrometry Imaging Reveals Distinct Accumulation Patterns of Steroid Structural Isomers in Human Adrenal Glands. *Anal Chem* **91**: 8918-8925.
34. Cobice, D. F., C. L. Mackay, R. J. Goodwin, A. McBride, P. R. Langridge-Smith, S. P. Webster, B. R. Walker, and R. Andrew. 2013. Mass spectrometry imaging for dissecting steroid intracrinology within target tissues. *Anal Chem* **85**: 11576-11584.
35. Shimma, S., H. O. Kumada, H. Taniguchi, A. Konno, I. Yao, K. Furuta, T. Matsuda, and S. Ito. 2016. Microscopic visualization of testosterone in mouse testis by use of imaging mass spectrometry. *Anal Bioanal Chem* **408**: 7607-7615.
36. Cobice, D. F., D. E. Livingstone, C. L. Mackay, R. J. Goodwin, L. B. Smith, B. R. Walker, and R. Andrew. 2016. Spatial Localization and Quantitation of Androgens in Mouse Testis by Mass Spectrometry Imaging. *Anal Chem* **88**: 10362-10367.
37. Zecchi, R., P. Franceschi, L. Tigli, D. Amidani, C. Catozzi, F. Ricci, F. Salomone, G. Pieraccini, B. Pioselli, and V. Mileo. 2021. Sample preparation strategy for the detection of steroid-like compounds using MALDI mass spectrometry imaging: pulmonary distribution of budesonide as a case study. *Anal Bioanal Chem* **413**: 4363-4371.
38. Barre, F. P., B. Flinders, J. P. Garcia, I. Jansen, L. R. Huizing, T. Porta, L. B. Creemers, R. M. Heeren, and B. Cillero-Pastor. 2016. Derivatization Strategies for the Detection of Triamcinolone Acetonide in Cartilage by Using Matrix-Assisted Laser Desorption/Ionization Mass Spectrometry Imaging. *Anal Chem* **88**: 12051-12059.
39. Mackay, C. L. L., J. Soltwisch, B. Heijs, K. W. Smith, F. L. Cruickshank, A. Nyhuis, K. Dreisewerd, and D. Cobice. 2021. Spatial distribution of isobaric androgens in target tissues using chemical derivatization and MALDI-2 on a trapped ion mobility quadrupole time-of-flight instrument. *RSC Adv* **11**: 33916-33925.
40. Cobice, D. F., D. E. W. Livingstone, A. McBride, C. L. MacKay, B. R. Walker, S. P. Webster, and R. Andrew. 2018. Quantification of 11beta-hydroxysteroid dehydrogenase 1 kinetics and pharmacodynamic effects of inhibitors in brain using mass spectrometry imaging and stable-isotope tracers in mice. *Biochem Pharmacol* **148**: 88-99.
41. Griffiths, W. J., Y. Wang, G. Alvelius, S. Liu, K. Bodin, and J. Sjovall. 2006. Analysis of oxysterols by electrospray tandem mass spectrometry. *J Am Soc Mass Spectrom* **17**: 341-362.
42. Roberg-Larsen, H., M. F. Strand, A. Grimsmo, P. A. Olsen, J. L. Dembinski, F. Rise, E. Lundanes, T. Greibrokk, S. Krauss, and S. R. Wilson. 2012. High sensitivity measurements of active oxysterols with automated filtration/filter backflush-solid phase extraction-liquid chromatography-mass spectrometry. *J Chromatogr A* **1255**: 291-297.
43. Yutuc, E., R. Angelini, M. Baumert, N. Mast, I. Pikuleva, J. Newton, M. R. Clench, D. O. F. Skibinski, O. W. Howell, Y. Wang, and W. J. Griffiths. 2020. Localization of sterols and oxysterols in mouse brain reveals distinct spatial cholesterol metabolism. *Proc Natl Acad Sci U S A* **117**: 5749-5760.
44. MacLachlan, J., A. T. Wotherspoon, R. O. Ansell, and C. J. Brooks. 2000. Cholesterol oxidase: sources, physical properties and analytical applications. *J Steroid Biochem Mol Biol* **72**: 169-195.
45. Lein, E. S., M. J. Hawrylycz, N. Ao, M. Ayres, A. Bensinger, A. Bernard, A. F. Boe, M. S. Boguski, K. S. Brockway, E. J. Byrnes, L. Chen, L. Chen, T. M. Chen, M. C. Chin, J. Chong, B. E. Crook, A. Czaplinska, C. N. Dang, S. Datta, N. R. Dee, A. L. Desaki, T. Desta, E. Diep, T. A. Dolbeare, M. J. Donelan, H. W. Dong, J. G. Dougherty, B. J. Duncan, A. J. Ebbert, G. Eichele, L. K. Estin, C. Faber, B. A. Facer, R. Fields, S. R. Fischer, T. P. Fliss, C. Frensley, S. N. Gates, K. J. Glattfelder, K. R. Halverson, M. R. Hart, J. G. Hohmann, M. P. Howell, D. P. Jeung, R. A. Johnson, P. T. Karr, R. Kawal, J. M. Kidney, R.

H. Knapik, C. L. Kuan, J. H. Lake, A. R. Laramee, K. D. Larsen, C. Lau, T. A. Lemon, A. J. Liang, Y. Liu, L. T. Luong, J. Michaels, J. J. Morgan, R. J. Morgan, M. T. Mortrud, N. F. Mosqueda, L. L. Ng, R. Ng, G. J. Orta, C. C. Overly, T. H. Pak, S. E. Parry, S. D. Pathak, O. C. Pearson, R. B. Puchalski, Z. L. Riley, H. R. Rockett, S. A. Rowland, J. J. Royall, M. J. Ruiz, N. R. Sarno, K. Schaffnit, N. V. Shapovalova, T. Sivisay, C. R. Slaughterbeck, S. C. Smith, K. A. Smith, B. I. Smith, A. J. Sodt, N. N. Stewart, K. R. Stumpf, S. M. Sunkin, M. Sutram, A. Tam, C. D. Teemer, C. Thaller, C. L. Thompson, L. R. Varnam, A. Visel, R. M. Whitlock, P. E. Wohnoutka, C. K. Wolkey, V. Y. Wong, M. Wood, M. B. Yaylaoglu, R. C. Young, B. L. Youngstrom, X. F. Yuan, B. Zhang, T. A. Zwingman, and A. R. Jones. 2007. Genome-wide atlas of gene expression in the adult mouse brain. *Nature* **445**: 168-176.

46. Yutuc, E., A. L. Dickson, M. Pacciarini, L. Griffiths, P. R. S. Baker, L. Connell, A. Öhman, L. Forsgren, M. Trupp, S. Vilarinho, Y. Khalil, P. T. Clayton, S. Sari, B. Dalgic, P. Höflinger, L. Schöls, W. J. Griffiths, and Y. Wang. 2021. Deep mining of oxysterols and cholestenoic acids in human plasma and cerebrospinal fluid: Quantification using isotope dilution mass spectrometry. *Anal Chim Acta* **1154**: 338259.

47. Kirkwood, K. I., M. T. Odenkirk, and E. S. Baker. 2023. Ion Mobility Spectrometry. *In* Mass Spectrometry for Lipidomics. 151-182.

48. Haider, A., C. Zhao, L. Wang, Z. Xiao, J. Rong, X. Xia, Z. Chen, S. K. Pfister, N. Mast, E. Yutuc, J. Chen, Y. Li, T. Shao, G. I. Warnock, A. Dawoud, T. R. Connors, D. H. Oakley, H. Wei, J. Wang, Z. Zheng, H. Xu, A. T. Davenport, J. B. Daunais, R. S. Van, Y. Shao, Y. Wang, M. R. Zhang, C. Gebhard, I. Pikuleva, A. I. Levey, W. J. Griffiths, and S. H. Liang. 2022. Assessment of cholesterol homeostasis in the living human brain. *Sci Transl Med* **14**: eadc9967.

49. Wang, L., Q. Zang, Y. Zhu, J. Liu, X. Li, X. Tu, X. Li, Z. Abliz, and R. Zhang. 2023. On-Tissue Chemical Oxidation Followed by Derivatization for Mass Spectrometry Imaging Enables Visualization of Primary and Secondary Hydroxyl-Containing Metabolites in Biological Tissues. *Analytical Chemistry* **95**: 1975-1984.

50. Wu, C., D. R. Ifa, N. E. Manicke, and R. G. Cooks. 2009. Rapid, direct analysis of cholesterol by charge labeling in reactive desorption electrospray ionization. *Anal Chem* **81**: 7618-7624.

51. Frisz, J. F., H. A. Klitzing, K. Lou, I. D. Hutcheon, P. K. Weber, J. Zimmerberg, and M. L. Kraft. 2013. Sphingolipid domains in the plasma membranes of fibroblasts are not enriched with cholesterol. *J Biol Chem* **288**: 16855-16861.

52. Lingwood, D., and K. Simons. 2010. Lipid rafts as a membrane-organizing principle. *Science* **327**: 46-50.

53. Corder, E. H., A. M. Saunders, W. J. Strittmatter, D. E. Schmechel, P. C. Gaskell, G. W. Small, A. D. Roses, J. L. Haines, and M. A. Pericak-Vance. 1993. Gene dose of apolipoprotein E type 4 allele and the risk of Alzheimer's disease in late onset families. *Science* **261**: 921-923.

54. Valenza, M., D. Rigamonti, D. Goffredo, C. Zuccato, S. Fenu, L. Jamot, A. Strand, A. Tarditi, B. Woodman, M. Racchi, C. Mariotti, S. Di Donato, A. Corsini, G. Bates, R. Pruss, J. M. Olson, S. Sipione, M. Tartari, and E. Cattaneo. 2005. Dysfunction of the cholesterol biosynthetic pathway in Huntington's disease. *J Neurosci* **25**: 9932-9939.

55. Wang, K., Z. Luo, C. Li, X. Huang, E. J. Shiroma, E. M. Simonsick, and H. Chen. 2021. Blood Cholesterol Decreases as Parkinson's Disease Develops and Progresses. *J Parkinsons Dis* **11**: 1177-1186.

56. Crick, P. J., W. J. Griffiths, J. Zhang, M. Beibel, J. Abdel-Khalik, J. Kuhle, A. W. Sailer, and Y. Wang. 2017. Reduced Plasma Levels of 25-Hydroxycholesterol and Increased Cerebrospinal Fluid Levels of Bile Acid Precursors in Multiple Sclerosis Patients. *Mol Neurobiol* **54**: 8009-8020.

57. Abdel-Khalik, J., E. Yutuc, P. J. Crick, J. A. Gustafsson, M. Warner, G. Roman, K. Talbot, E. Gray, W. J. Griffiths, M. R. Turner, and Y. Wang. 2017. Defective cholesterol metabolism in amyotrophic lateral sclerosis. *J Lipid Res* **58**: 267-278.

58. Wang, Y., E. Yutuc, and W. J. Griffiths. 2021. Neuro-oxysterols and neuro-sterols as ligands to nuclear receptors, GPCRs, ligand-gated ion channels and other protein receptors. *Br J Pharmacol* **178**: 3176-3193.

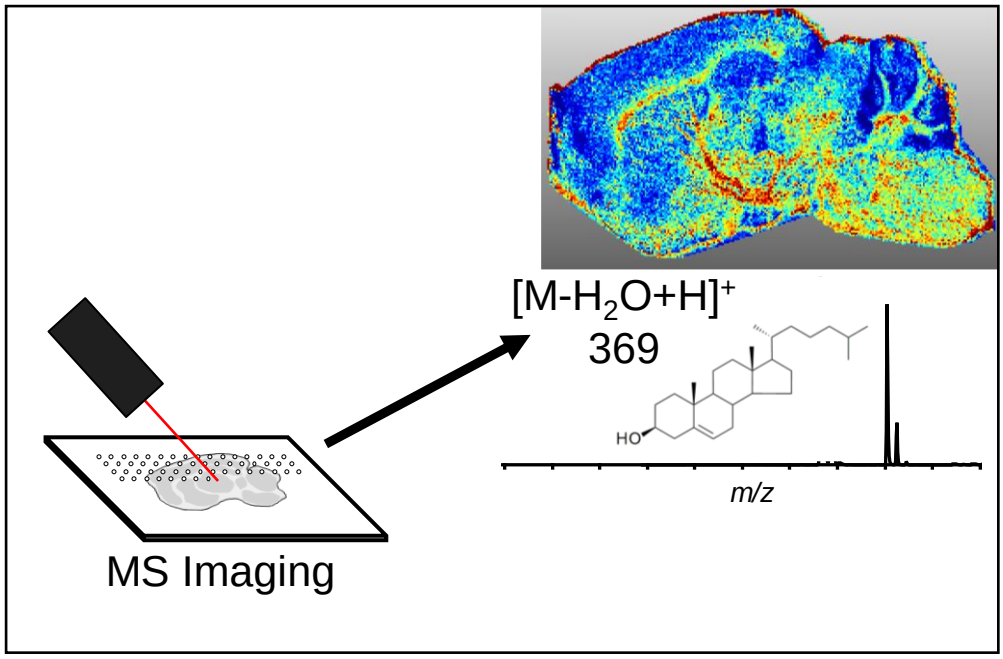

Figure 1.

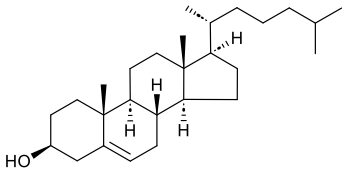

Cholesterol
Chemical Formula: $C_{27}H_{46}O$
Exact Mass: 386.3549

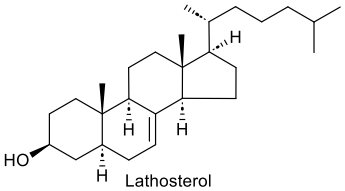

Lathosterol
Chemical Formula: $C_{27}H_{46}O$
Exact Mass: 386.3549

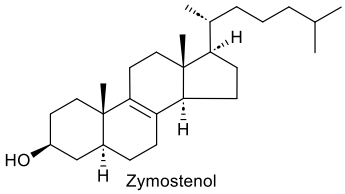

Zymostenol
Chemical Formula: $C_{27}H_{46}O$
Exact Mass: 386.3549

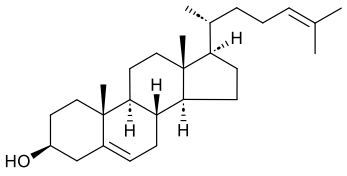

Desmosterol
Chemical Formula: $C_{27}H_{44}O$
Exact Mass: 384.3392

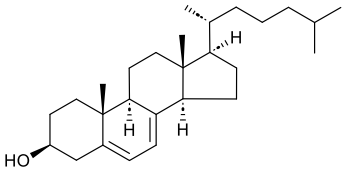

7-Dehydrocholesterol
Chemical Formula: $C_{27}H_{44}O$
Exact Mass: 384.3392

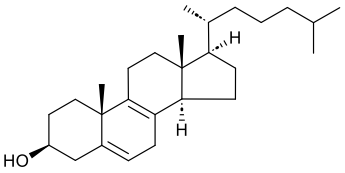

8-Dehydrocholesterol
Chemical Formula: $C_{27}H_{44}O$
Exact Mass: 384.3392

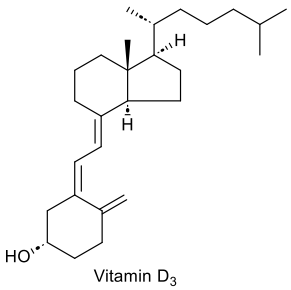

Vitamin D_3
Chemical Formula: $C_{27}H_{44}O$
Exact Mass: 384.3392

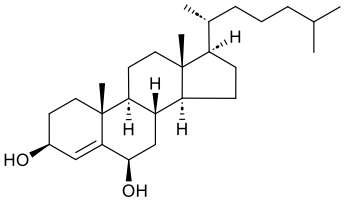

6β-Hydroxycholesterol
Chemical Formula: $C_{27}H_{46}O_2$
Exact Mass: 402.3498

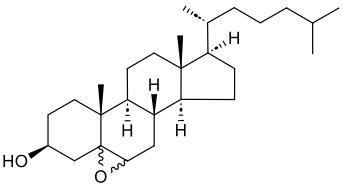

Cholesta-5.6-epoxide
Chemical Formula: $C_{27}H_{46}O_2$
Exact Mass: 402.3498

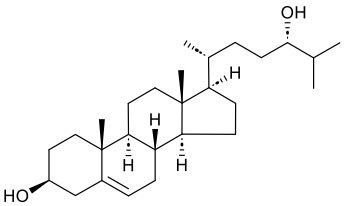

24S-Hydroxycholesterol
Chemical Formula: $C_{27}H_{46}O_2$
Exact Mass: 402.3498

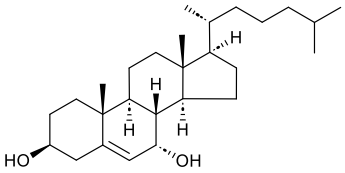

7α-Hydroxycholesterol
Chemical Formula: $C_{27}H_{46}O_2$
Exact Mass: 402.3498

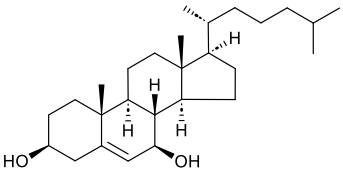

7β-Hydroxycholesterol
Chemical Formula: $C_{27}H_{46}O_2$
Exact Mass: 402.3498

Figure 2.

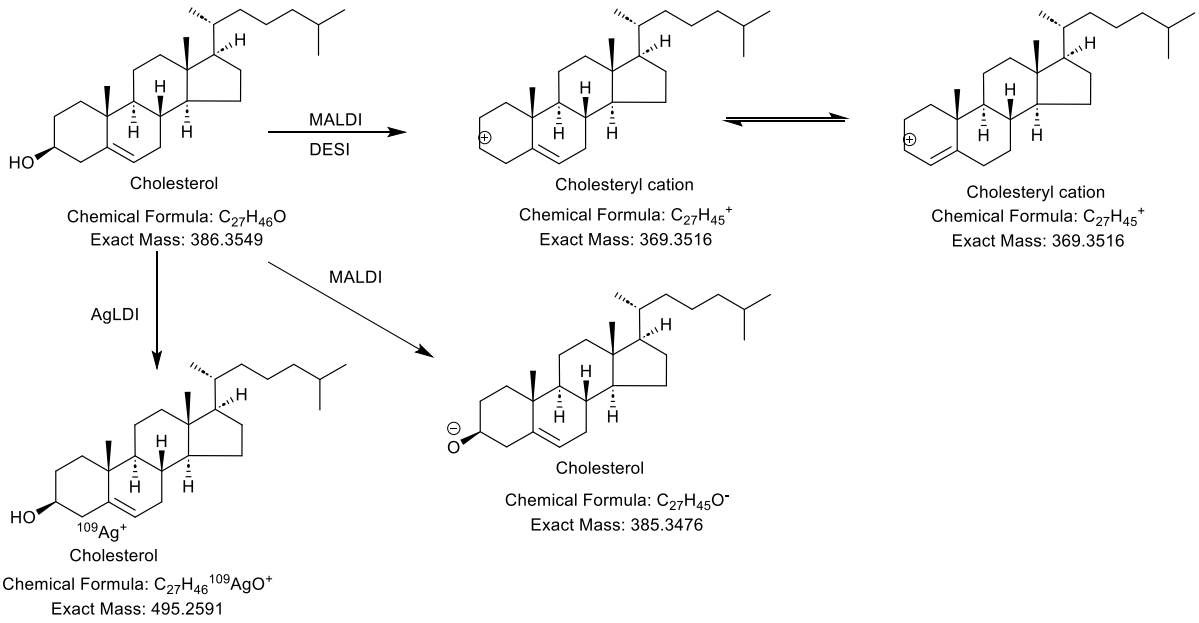
MALDI
DESI
Cholesterol
Chemical Formula: C27H46O
Exact Mass: 386.3549
Cholesteryl cation
Chemical Formula: C27H45+
Exact Mass: 369.3516
Cholesteryl cation
Chemical Formula: C27H45+
Exact Mass: 369.3516
AgLDI
MALDI
Cholesterol
Chemical Formula: C27H45O-
Exact Mass: 385.3476
109Ag+
Cholesterol
Chemical Formula: C27H46109AgO+
Exact Mass: 495.2591

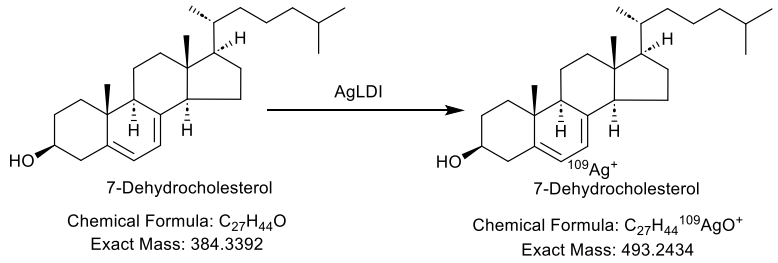
AgLDI
7-Dehydrocholesterol
Chemical Formula: C27H44O
Exact Mass: 384.3392
109Ag+
7-Dehydrocholesterol
Chemical Formula: C27H44109AgO+
Exact Mass: 493.2434

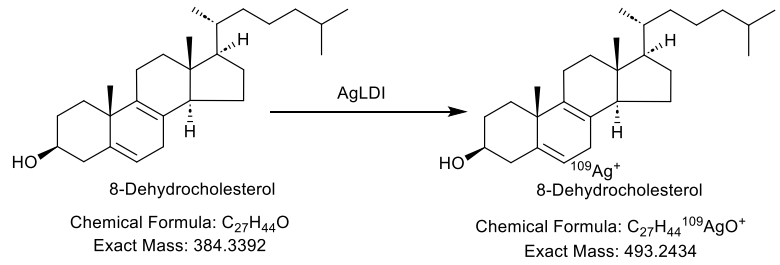
AgLDI
8-Dehydrocholesterol
Chemical Formula: C27H44O
Exact Mass: 384.3392
109Ag+
8-Dehydrocholesterol
Chemical Formula: C27H44109AgO+
Exact Mass: 493.2434

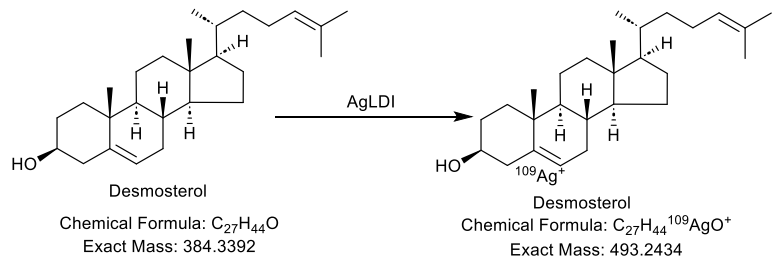
AgLDI
Desmosterol
Chemical Formula: C27H44O
Exact Mass: 384.3392
109Ag+
Desmosterol
Chemical Formula: C27H44109AgO+
Exact Mass: 493.2434

Figure 3.

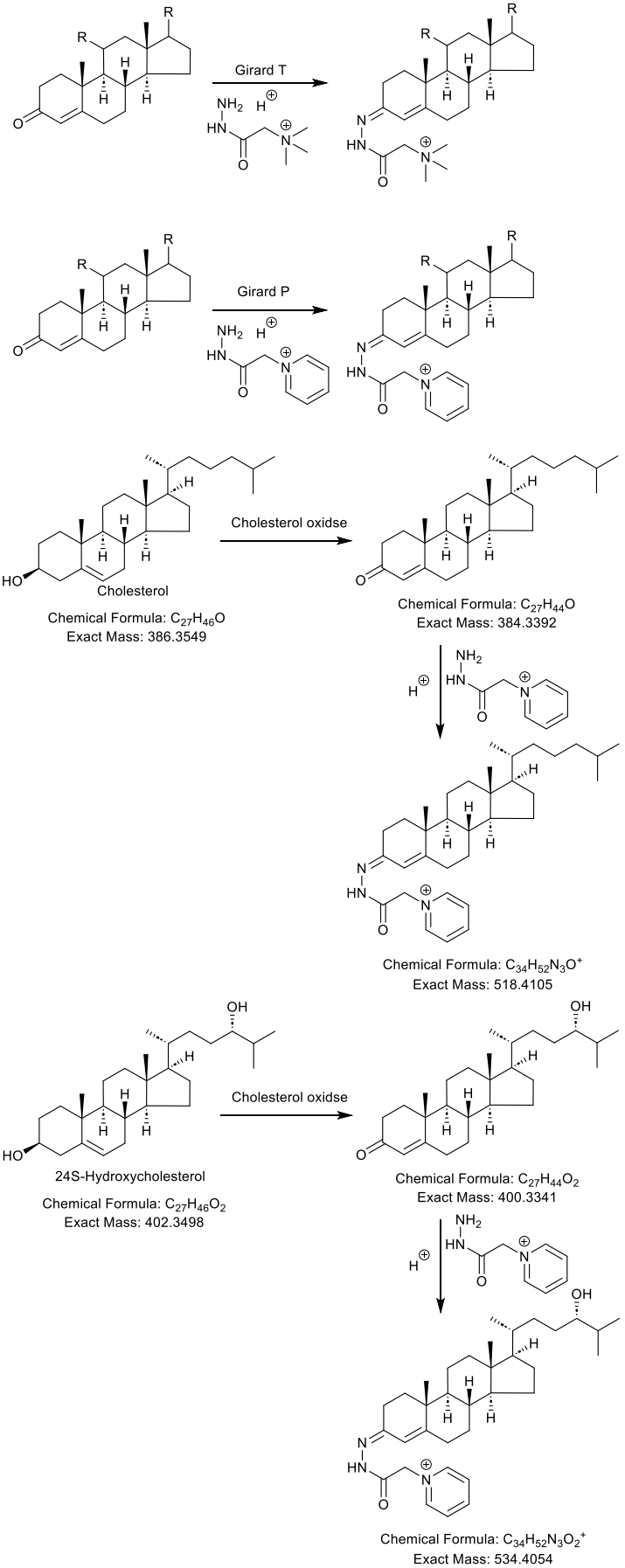
Girard T
Girard P
Cholesterol oxidse
Cholesterol
Chemical Formula: C27H46O
Exact Mass: 386.3549
Chemical Formula: C27H44O
Exact Mass: 384.3392
Chemical Formula: C34H52N3O+
Exact Mass: 518.4105
24S-Hydroxycholesterol
Chemical Formula: C27H46O2
Exact Mass: 402.3498
Chemical Formula: C27H44O2
Exact Mass: 400.3341
Chemical Formula: C34H52N3O2+
Exact Mass: 534.4054

Figure 4.

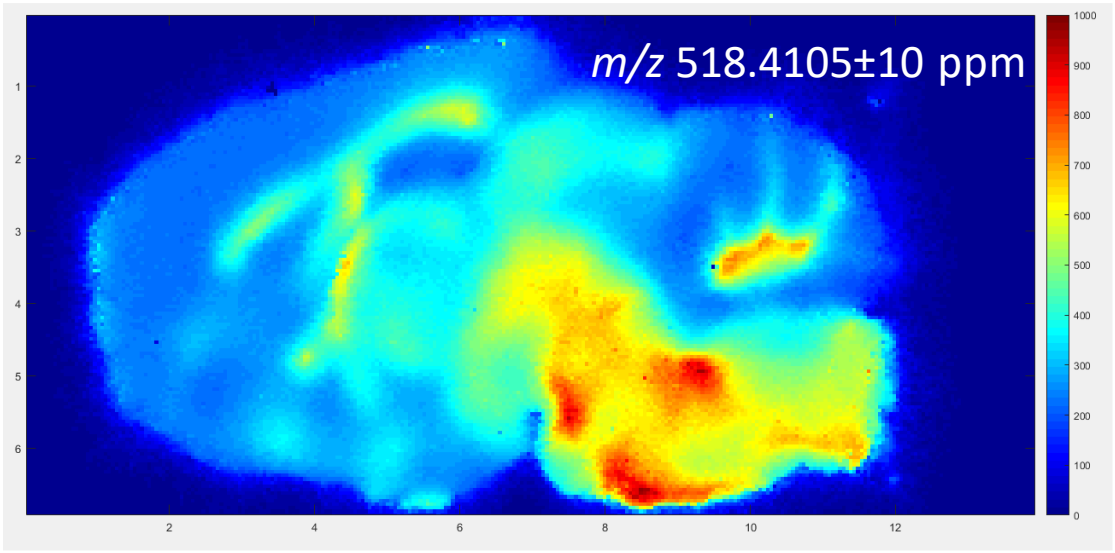
m/z 518.4105±10 ppm
1000
900
800
700
600
500
400
300
200
100
0
ng/mm2

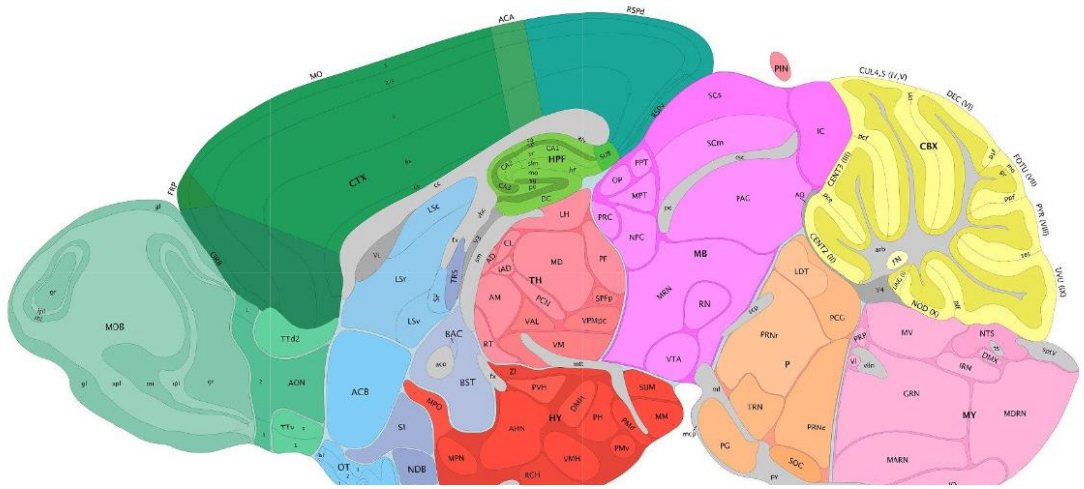
ACA
RSPd
MO
PIN
CUL4,5 (V,X)
DEC (IX)
SCs
SCm
IC
CBX
CENT3 (III)
CENT2 (II)
FOTU (VIII)
PYR (VIII)
UVU (IX)
NOD (X)
CTX
HPF
FPT
OM
MPT
PAG
LH
PRC
NPC
MB
LDT
PRNr
PCG
P
MV
NTS
DMX
IRN
GRN
MY
MDRN
MARN
TRN
PRNc
PG
SOC
MOB
TTd2
AON
ACB
BAC
BST
LSr
LSv
LSc
TRS
CL
AD
iAD
MD
PF
TH
AM
PCN
VAL
SPFp
VPMdc
RT
VM
MRN
RN
VTA
ZI
PVH
HY
AHN
DMH
PH
PMd
SUM
MM
PMv
MPN
VMH
RCH
MPO
SI
OT
NDB

Figure 5.

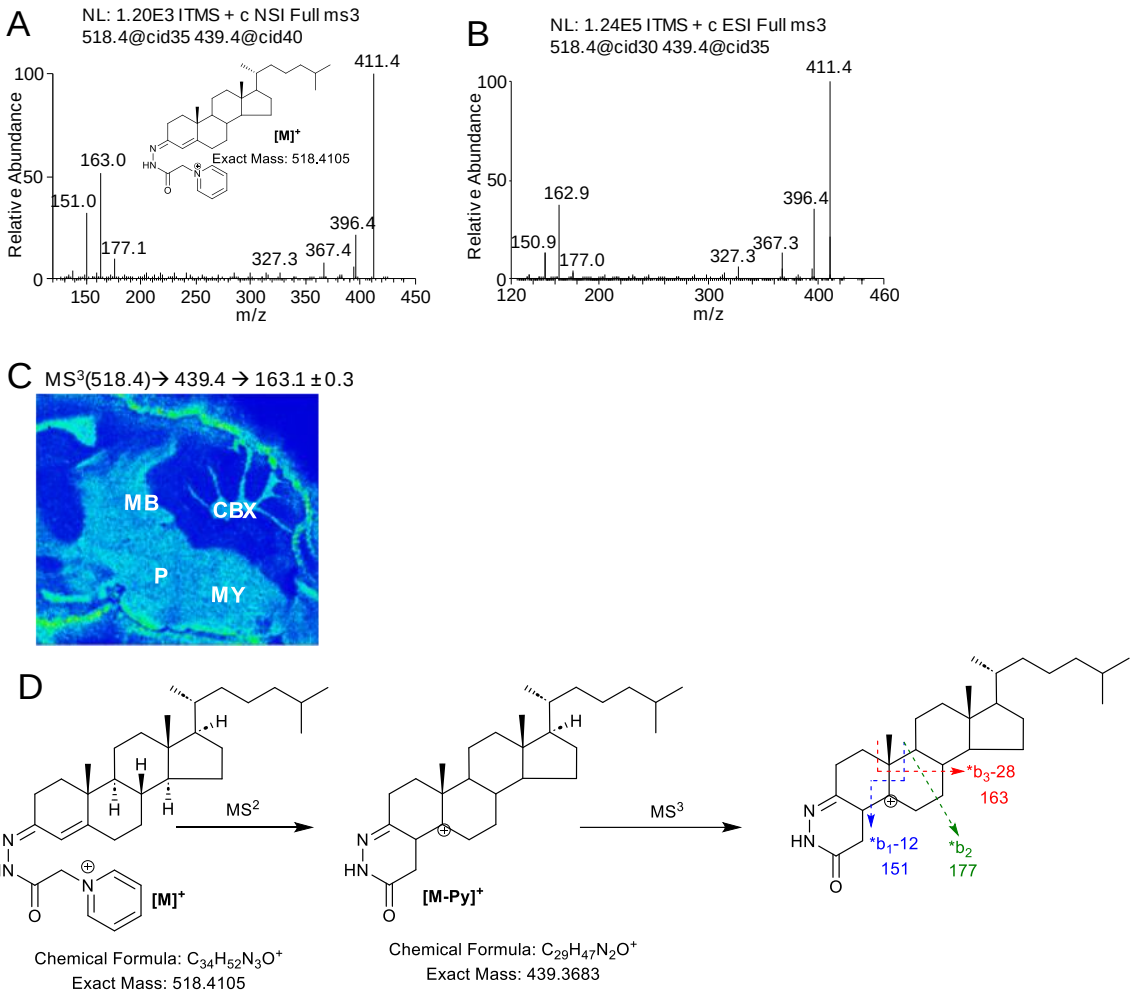
A
NL: 1.20E3 ITMS + c NSI Full ms3
518.4@cid35 439.4@cid40
Relative Abundance
m/z
411.4
163.0
151.0
177.1
327.3
367.4
396.4
[M]+
Exact Mass: 518.4105
B
NL: 1.24E5 ITMS + c ESI Full ms3
518.4@cid30 439.4@cid35
411.4
162.9
150.9
177.0
327.3
367.3
396.4
C
MS3(518.4)→ 439.4 → 163.1 ±0.3
MB
CBX
P
MY
D
MS2
MS3
[M]+
[M-Py]+
*b3-28
163
*b1-12
151
*b2
177
Chemical Formula: C34H52N3O+
Exact Mass: 518.4105
Chemical Formula: C29H47N2O+
Exact Mass: 439.3683

Figure 6.

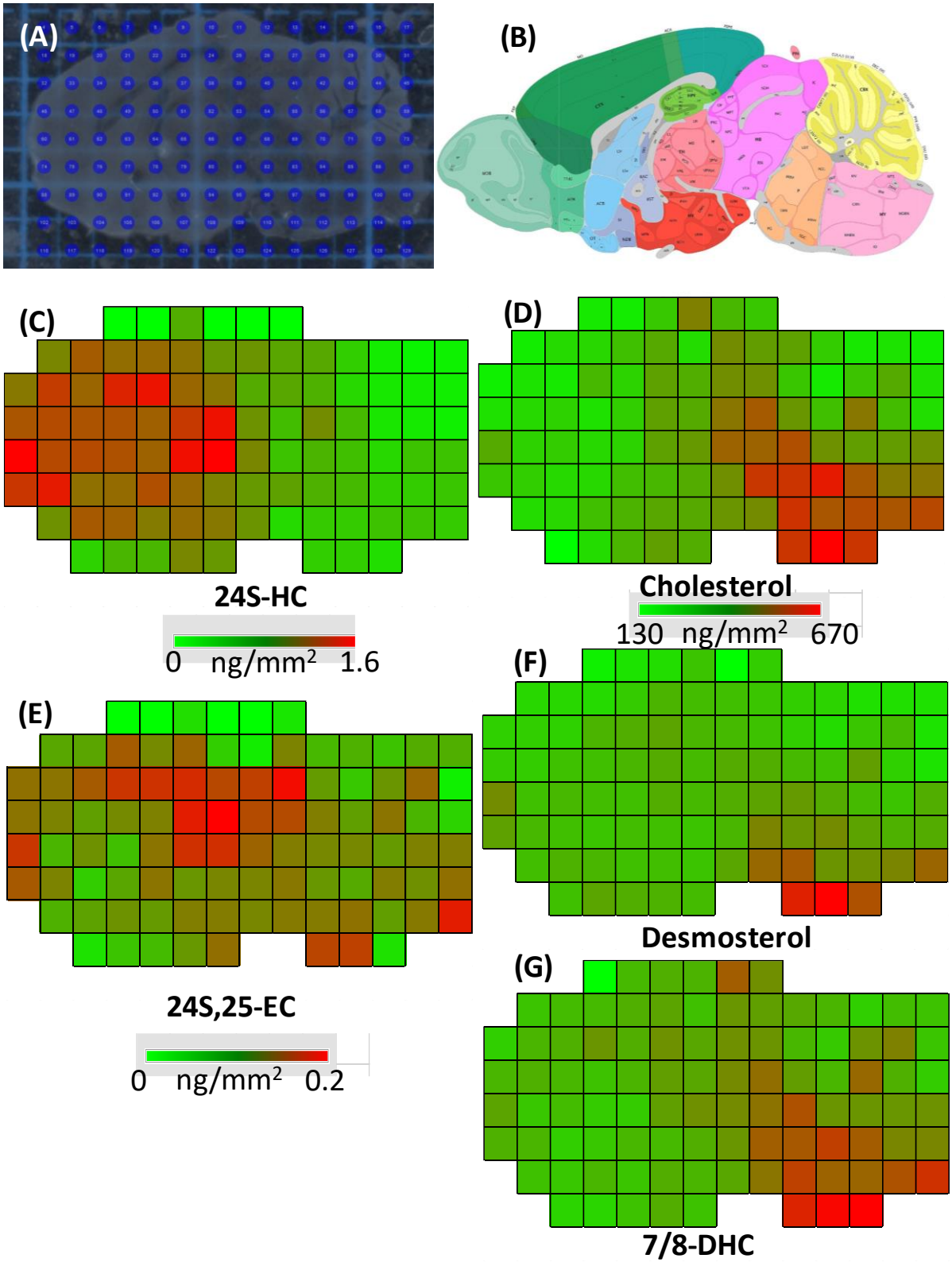
(A)
(B)
(C)
24S-HC
0 ng/mm2 1.6
(D)
Cholesterol
130 ng/mm2 670
(E)
24S,25-EC
0 ng/mm2 0.2
(F)
Desmosterol
(G)
7/8-DHC

Figure 7.